Proceedings of ASME Turbo Expo 2014: Turbine Technical Conference and Exposition
GT2014
June 16-20, 2014, Düsseldorf, Germany

DOI: 10.1115/GT2014-25224

GT2014-25224

SCALING METHODS FOR MATCHING TASKS IN TURBOCHARGED ENGINES

Thibaut Njoya
Industrial Science GmbH
Alexanderstraße 25,
64287 Darmstadt, Germany
Email: thibaut.njoya@industrial-science.de

Mehdi Nakhjiri
Industrial Science GmbH
Alexanderstraße 25,
64287 Darmstadt, Germany
Email: mehdi.nakhjiri@industrial-science.de

Peter F. Pelz
Chair of Fluid Systems
Technische Universität Darmstadt,
Magdalenenstraße 4,
64287 Darmstadt, Germany
Email: peter.pelz@fst.tu-darmstadt.de

Robert Frase
IAV GmbH
Rockwellstraße 4,
38518 Gifhorn, Germany
Email: robert.frase@iav.de

ABSTRACT

Specific turbocharger parameters are necessary to develop and match model based control strategies in the air path of a turbocharged engine. These parameters describe the turbocharger performance and are obtained from measurements on manufacturers' standard test benches under steady state conditions and without taking into account the heat transfer between the components of the turbocharger or between the turbocharger and the surroundings. The latter falsifies the measured turbocharger efficiency which can be referred as "apparent efficiency". The efficiency is a key parameter of the model based controls. Thus, the apparent efficiency increases the uncertainties (mismatching) and slows down the matching process considerably.

Due to the mismatching, manufacturers' parameters themselves need to be calibrated. The calibration occurs on the basis of on-board measurements and offline analyses. However, this calibration procedure is not axiomatic and the results remain typical for a certain turbocharger and engine combination. Hence, it is usually not possible to apply the results when the same turbocharger should be matched with another engine.

A physically based scaling method has already been introduced in previous publications in order to obtain the "real" from the "apparent" efficiency, [1]. This work aims to show on the basis of a concrete example how the implementation of this method counteracts the mismatching without any further measurements. As a result, the matching process can be accelerated and enhanced. The reusability of the results leads to faster processes and lower costs.

NOMENCLATURE

c_p	specific heat capacity at constant pressure, J/kg K.
d	diameter, m.
h	specific enthalpy, J/kg.
$\dot{m}$	mass flow, kg/s.
p	pressure, Pa.
q	specific heat, J/kg
R	gas constant, J/kg K.
s	specific entropy, J/kg K.
T	temperature, K.
u	circumferential speed, m/s.
η	efficiency.
γ	isentropic exponent.
ρ	density, kg/m^3.
Π	pressure ratio.
φ	flow coefficient.

Subscripts

C	compressor.
O	overall.
is	isentropic.
T	turbine.
TM	combined, i.e. turbine and mechanical.
t	total, stagnation.
1	compressor inlet.
2	compressor outlet.
3	turbine inlet.
4	turbine outlet.

opt optimum.
ad adiabatic.
ref reference.

Superscripts

′ apparent, from manufacturers' maps.

INTRODUCTION

Turbochargers are generally measured on manufacturer's hot gas test stands. Due to the temperature differences between turbine, compressor and environment the heat flow during the operation of the turbocharger cannot be neglected. However, the control volume used by the manufacturer does not allow for heat flow phenomena. Therefore, the efficiency of compressor and turbine estimated on manufacturers' performance maps are inappropriate and should be referred to as apparent efficiencies, [1].

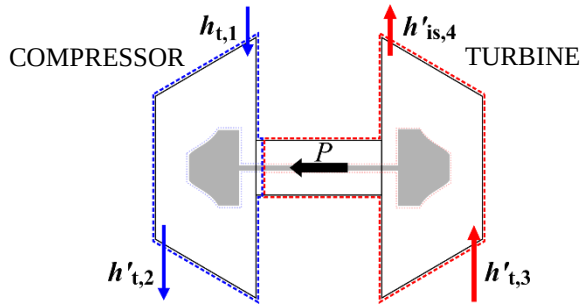

Figure 1. MEASURING PLANES OF A STANDARD MANUFACTURER'S TEST STAND.

Figure 1 shows the measuring planes of a manufacturer's test stand. Here, the performance of compressor and turbine are evaluated through measurements of the gas properties after the casing.

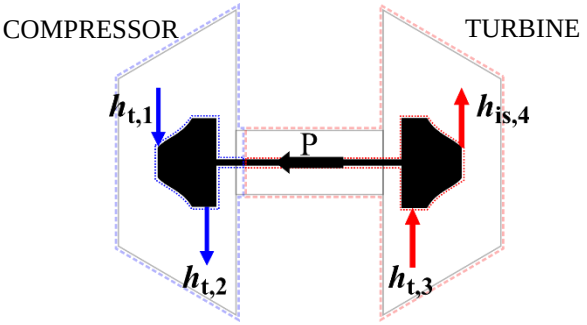

Figure 2. MEASURING PLANES OF AN OPTIMAL TEST STAND.

A test stand that is really appropriate to evaluate the performance turbo machine must involve measurements immediately before and after the rotors as illustrated in Figure 2. Figure 3 illustrates the difference between both. On the compressor side (with blue lines demarcated area) of a standard manufacturer's test stand, the outlet total enthalpy erroneously includes the heat flow from the hot casing to the fluid, apparently increasing the outlet total enthalpy, hence, the evaluated compressor input power. On the turbine side (with red lines demarcated area that usually includes both turbine and bearing housing), the heat transfer from the hot exhaust gas to the turbine casing before the rotor inlet is neglected. Therefore, the working capacity of the gas prior to expansion is apparently higher. The realization of a real test rig that matches Figure 2 is practically impossible due to the poor accessibility of the measuring planes. Hence, there is a need to compute the real values out of Figure 2 from the apparent values out of Figure 1.

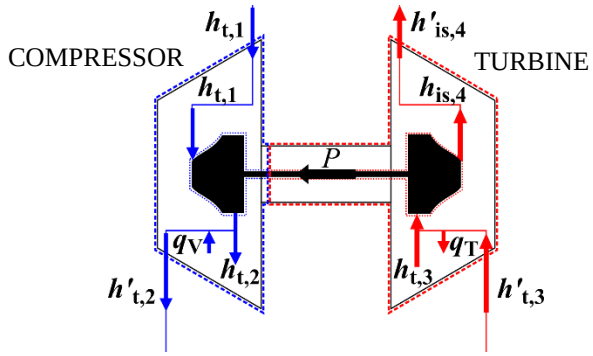

Figure 3. DIFFERENCES BETWEEN MANUFACTURER'S AND OPTIMAL TEST STAND.

To meet the requirements of modern engines regarding the fast adjustment of the manifold pressure, recent developments focus on physically based control strategies to regulate the air path of turbocharged engines, thereby reducing the parameterization effort for a different combination of engine and turbocharger. The turbocharger's efficiency is a key parameter to develop and match the physically based model. However, the apparent efficiency from manufacturer's maps increases the uncertainties and leads to mismatching. Thus, a costly and time consuming process is required to calibrate the manufacturer's maps themselves. Other sources of uncertainties have been investigated in [16] and [17].

In fact, both the calibration of the manufacturer's parameters and the matching of the physically based control model occur simultaneously on the basis of on-board measurements and offline analysis. The calibration process starts with the available manufacturer's maps. Then the maps are adjusted manually on the basis of systematical test cycles and offline analyses of the test results until a good match to the desired boost pressure is achieved. This procedure is not axiomatic and does not exploit the full potential of the physical model by increasing the parameterization effort. Therefore, the results remain typical for a certain turbocharger and engine combination and it may not be possible to apply the calibrated manufacturer's parameter when the same turbocharger should be matched with another engine. Hence, to take advantage of physically based control strategies it is necessary to feed the model with adequate parameters that describe the real performance of the machine.

In recent years many research papers have focused on models to estimate the amount of heat flow in a turbocharger thus, allowing an estimation of the real efficiency of the turbo machine; see [2, 3, 4, 5, 6, 7, 8] and many references given in these publications. Some models such as those described in [2]

and [3] specify Nusselt relations to quantify the heat flow, others are based on the analysis of the turbocharger's characteristic variables such as the power coefficient [4]. However, simplicity is required for an industrial application of these methods.

In this paper, a method which is suitable for an industrial application and allows retrieving the real compressor and turbine maps out of the manufacturer's (apparent) ones is used to counteract the heat transfer effects in a small passenger car turbocharger. It is based on the scaling method presented previously in [1]. It is then shown from vehicle measurements how this method contributes to speed up the matching process.

SCALING COMPRESSOR MAPS FROM APPARENT TO REAL EFFICIENCY

The scaling method for the compressor is based on the fact that the heat flux through the compressor causes a drop in the efficiency at low shaft speeds and is illustrated in Figure 4. There is a linear correlation between the efficiency and flow coefficient at optimum in turbo machines that has been proven by previous researchers [9, 10, 11]. Previously, Nakhjiri et al. ([1]) have shown that this relation holds for turbochargers under adiabatic conditions with respect to the outlet flow coefficient. Due to the heat flow, the compressor efficiency optimum at low speeds lies under the correlation line and must be shifted to the latter while the outlet flow coefficient remains constant. This method is chosen because it is easy to apply and allows a fast and reliable way to determine the real compressor maps. Furthermore, no additional data other than those available on the common manufacturer's maps are required when using the proposed method.

Early investigations to understand the heat transfer effects on the turbocharger performance have shown that the heat transfer affects the efficiency of the turbocharger whereas the influence on the total pressure ratio between inlet and outlet is negligible, see [1, 8]. Therefore, it is assumed that the pressure ratio available in manufacturers' maps remains unchanged and the method used in this work corrects the efficiency maps.

In the following, it is assumed that the medium flowing through the compressor is an ideal gas and its inlet state is known. Manufacturer's compressor maps include the total pressure ratio

$$\Pi_{\mathrm{tC}} = \frac{p_{\mathrm{t2}}}{p_{\mathrm{t1}}} \tag{1}$$

and the apparent efficiency (marked by a dash)

$$\eta'_{\mathrm{C}} = \frac{\Delta h_{\mathrm{t,is,C}}}{\Delta h'_{\mathrm{t,C}}} \tag{2}$$

as function of the shaft rotational speed and the mass flow through the machine. The total density of the compressed gas is approximately given by

$$\rho'_{\mathrm{t2}} = \frac{p_{\mathrm{t1}}}{R T_{\mathrm{t1}}} \frac{\Pi_{\mathrm{tC}}}{1 + \dfrac{\Pi_{\mathrm{tC}}^{(\gamma-1)/\gamma} - 1}{\eta'_{\mathrm{C}}}}, \tag{3}$$

assuming that the specific heat capacity at constant pressure c_p is roughly constant. The outlet flow coefficient is estimated using the stagnation state at the rotor outlet according to

$$\varphi'_2 = \frac{\dot{m}_{\mathrm{C}}}{\rho'_{\mathrm{t2}} u_2 \pi d_2^2/4} \approx \varphi_2 \,. \tag{4}$$

An investigation of the effect of the heat addition on the outlet flow coefficient has shown negligible discrepancies between the real and the apparent flow coefficient.

The compressor efficiency is then plotted against the outlet flow coefficient as shown in Figure 4 for the investigated turbocharger. At high shaft rotational speed, the heat flux effects are negligible. Thus, a connection line

$$\eta_{\mathrm{C,opt}} = a + b\varphi_{2,\mathrm{opt}} \,, \tag{5}$$

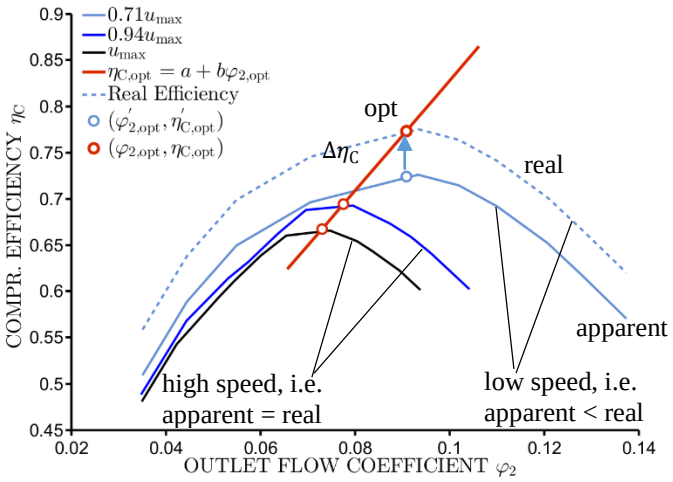

Figure 4. APPLICATION OF THE SCALING METHOD ON THE EFFICIENCY MAP OF A COMPRESSOR.

is fitted relative to the coefficients a and b using the peaks of both efficiency curves with the highest shaft speed. This corresponds to the red line in Figure 4. All curves with peaks under the correlation line must be shifted up vertically back to this line. The magnitude of the shift is given by the difference between the real (red circled point in Figure 4) and the apparent efficiency's optimum (blue circled point in Figure 4), i.e.

$$\begin{aligned} \Delta\eta_{\mathrm{C}} &= \eta_{\mathrm{C,opt}} - \eta'_{\mathrm{C,opt}} \,, \\ \eta_{\mathrm{C}} &= \eta'_{\mathrm{C}} + \Delta\eta_{\mathrm{C}} \,. \end{aligned} \tag{6}$$

The real value of the compressor input work is now

$$\Delta h_{\mathrm{t,C}} = h_{\mathrm{t1}} \frac{\Pi_{\mathrm{tC}}^{\frac{\gamma-1}{\gamma}} - 1}{\eta_{\mathrm{C}}} \,. \tag{7}$$

It is lower than the apparent compressor input work from the manufacturer's compressor efficiency map

$$\Delta h'_{\mathrm{t,C}} = h_{\mathrm{t1}} \frac{\Pi_{\mathrm{tC}}^{\frac{\gamma-1}{\gamma}} - 1}{\eta'_{\mathrm{C}}} \tag{8}$$

since the real efficiency η_C is higher than the apparent η'_C.

SCALING TURBINE MAPS FROM APPARENT TO REAL EFFICIENCY

The Turbine maps include the reduced turbine mass flow

$$\dot{m}_{\mathrm{red,T}} = \dot{m}_T \frac{\sqrt{T_{t3}}}{p_{t3}}$$

and the turbine efficiency as function of the total to static pressure ratio and the shaft speed

$$\Pi_T = \frac{p_{t3}}{p_4}.$$

As for the compressor it has been proven that heat transfer on the turbine side has negligible effects on the pressure ratio through the turbine rotor but affects the combined efficiency, see [1, 8].

Generally, the mechanical losses in the bearing housing are combined with the aerodynamic losses in the turbine rotor to a combined turbine efficiency which is referred to as combined efficiency below. The output power of the combined system is equivalent to the input power of the compressor. Therefore, the combined efficiency reads the ratio of the compressor input power to the turbine input power, i.e. (in the case of the apparent combined efficiency)

$$\eta'_{TM} := \frac{\dot{m}_C \Delta h'_{t,C}}{\dot{m}_T \Delta h'_{t,is,T}}. \quad (9)$$

The latter expression corresponds to the apparent manufacturer's combined efficiency. It includes the apparent combined system output work which is equivalent to the apparent compressor input work $\dot{m}_C \Delta h'_{t,C}$. As illustrated in Figure 3, the heat transfer that takes place prior to the expansion in the turbine rotor is ignored in manufacturer's test stand. Hence, the manufacturer's efficiency reads the apparent turbine input work $\Delta h'_{t,is,T}$ (Eqn. (9)).

To compute the real combined efficiency, both the real compressor input work and the real turbine input work have to be determined. Therefore, two steps are needed for this aim. First of all, the results from the previous section are used to compute the adiabatic combined efficiency that takes the real output work of the combined system into account, i.e.

$$\eta_{TM,ad} := \frac{\dot{m}_C \Delta h_{t,C}}{\dot{m}_T \Delta h'_{t,is,T}}. \quad (10)$$

Then, the real combined efficiency that takes into account the real turbine input work is computed, assuming that the correction of the apparent turbine input work to the real one leads to a positive shift from the adiabatic combined efficiency to the real combined efficiency, i.e.

$$\eta_{TM} := \frac{\dot{m}_C \Delta h_{t,C}}{\dot{m}_T \Delta h_{t,is,T}} = \eta_{TM,ad} + \Delta\eta_{TM}, \quad (11)$$

where $\Delta\eta_{TM}$ represents the magnitude of the shift. The argumentation for these steps is detailed hereafter.

FIRST STEP: FROM APPARENT TO ADIABATIC COMBINED EFFICIENCY

First, the numerator of Eqn. (9) is corrected, leading to the adiabatic combined efficiency. The Term adiabatic in this step refers to the fact that the stagnation enthalpy downstream (upstream) of the rotor and downstream (upstream) of the stage are equal for the compressor (turbine) as illustrated in Figure 5. Therefore it is assumed that the change of state between these two measuring planes is adiabatic. Since an adiabatic change of state has been assumed in the rotor, the change of state in the whole stage is adiabatic. In this step the adiabatic overall efficiency is introduced, that takes the real compressor efficiency computed using the scaling method into account. Thus, the apparent power addition to the compressor flow through heat is corrected and the stagnation enthalpy at the compressor stage outlet is equivalent to that at the rotor outlet. On the other side the denominator of Eqn. (9) remains unchanged, maintaining the assumption from the manufacturer's test stand that the stagnation enthalpy at the turbine rotor inlet is equal to that at stage inlet.

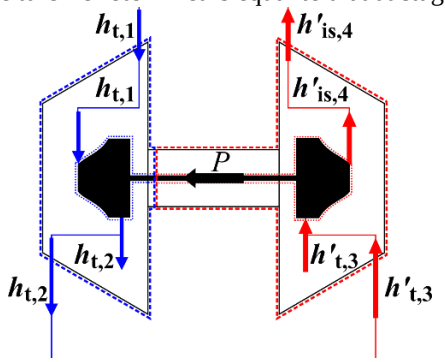

Figure 5. ADIABATIC TEST STAND.

The apparent overall efficiency from manufacturers' maps is

$$\eta'_O := \eta'_C \eta'_{TM} = \frac{\dot{m}_C \Delta h_{t,is,C}}{\dot{m}_T \Delta h'_{t,is,T}}, \quad (12)$$

whereas the following equation holds for the adiabatic overall efficiency

$$\eta_{O,ad} := \eta_C \eta_{TM,ad} = \frac{\dot{m}_C \Delta h_{t,is,C}}{\dot{m}_T \Delta h'_{t,is,T}} = \eta'_O. \quad (13)$$

When comparing the right side of Eqn. (12) and Eqn. (13) it comes out that the apparent and the adiabatic efficiency are equal. Therefore, it is possible to solve Eqn. (13) for the adiabatic combined efficiency, i.e.

$$\eta_{TM,ad} = \frac{\eta'_O}{\eta_C} = \frac{\dot{m}_C \Delta h_{t,C}}{\dot{m}_T \Delta h'_{t,is,T}}. \quad (14)$$

Figure 6 compares the apparent (solid lines) and the adiabatic (dashed lines) combined efficiency. At high speed where the heat transfer effects on compressor are negligible both turbine efficiencies are equal. At lower speeds with significant

influence of heat on the evaluated compressor performance the adiabatic efficiency is lower. The higher the shaft speed, the higher the combined efficiency. This result for the adiabatic combined efficiency is related to the Reynolds-dependency of the mechanical efficiency whose pattern dominates that of the single turbine efficiency when combining both. The dimensionless mechanical losses are higher at lower shaft speeds according to the Colebrook diagram. The latter is also in agreement with the experimental results in [12] where the mechanical efficiency is higher at higher shaft Reynolds number for an adiabatic turbocharger. This is also true for a turbocharger under the influence of heat flow phenomena. At higher speeds, more heat is supplied to the bearing housing thus, reducing the viscosity of the oil and increasing the Reynolds number.

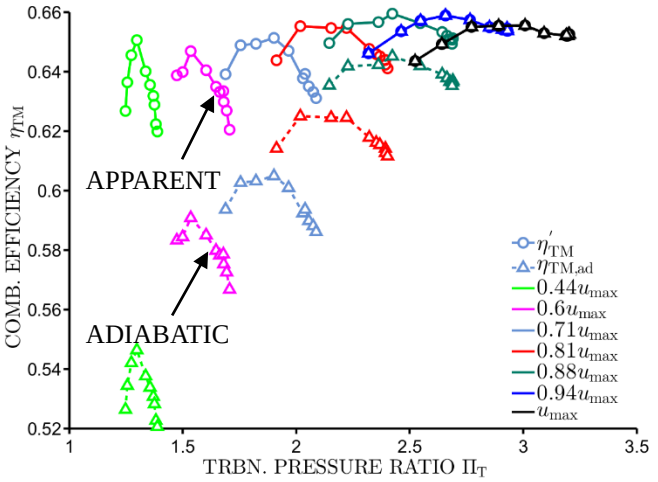

Figure 6. COMPARISON OF APPARENT AND ADIABATIC COMBINED EFFICIENCY.

SECOND STEP: FROM ADIABATIC TO REAL COMBINED EFFICIENCY

Second, the denominator of Eqn. (9) is corrected, taking the heat transfer effects on the turbine into account and leading to the real combined efficiency.

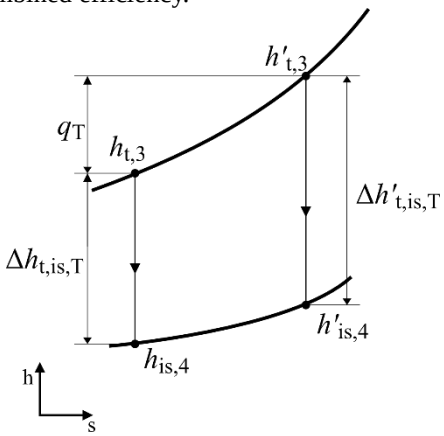

Figure 7. APPARENT AND REAL TURBINE ISENTROPIC CHANGE OF STATE.

In the previous step, based on the manufacturer's test stand, the latter has been neglected and it was assumed that the change of total enthalpy only occurs in the turbine rotor. In a real test stand, heat is conducted from the hot gas before entry in the rotor through the turbine casing to the surroundings. The heat loss decreases the total enthalpy of the exhaust gas prior to expansion in the rotor. As a result, the work capacity of the fluid is reduced and due to the spread of the isobar lines the real isentropic change of state is lower than the apparent, i.e. $\Delta h_{t,is,T} < \Delta h'_{t,is,T}$ as shown in Figure 7. This leads according to definition to a higher real combined efficiency in comparison to the adiabatic, i.e.

$$\eta_{TM} = \eta_{TM,ad} + \Delta\eta_{TM}\,, \tag{15}$$

where $\Delta\eta_{TM}$ is strictly positive and represents the shift from the adiabatic to the real combined efficiency. There is one issue about this increase that simplifies the estimation of the real efficiency: the magnitude of the shift from adiabatic to real efficiency is nearly constant at all shaft speeds for a given turbocharger. This assumption is discussed in the following.

According to the definition of the real combined efficiency (see Eqn. (11)), the combined efficiency shift is given by

$$\Delta\eta_{TM} = \underbrace{\frac{\dot{m}_C \Delta h_{t,C}}{\dot{m}_T \Delta h'_{t,is,T}}}_{(1)} \underbrace{\frac{\Delta h'_{t,is,T} - \Delta h_{t,is,T}}{\Delta h_{t,is,T}}}_{(2)}\,. \tag{16}$$

The left quotient of Eqn. (16) is equivalent to the adiabatic combined efficiency which is higher at higher shaft speeds. The right quotient depends on the amount of the supplied specific heat. Assuming that the exhaust gas is an ideal gas and the heat capacity is roughly constant, the isentropic change of state is given by

$$\Delta h_{t,is,T} = h_{t,3}\left(1 - \Pi_T^{-\frac{\gamma-1}{\gamma}}\right). \tag{17}$$

Since the difference between the apparent and the real total enthalpy is the amount of heat dissipated,

$$h_{t,3} = h'_{t,3} - q_T\,,$$

the right quotient of Eqn. (16), the relative change of the isentropic work between real and apparent, yields

$$\frac{\Delta h'_{t,is,T} - \Delta h_{t,is,T}}{\Delta h_{t,is,T}} = \frac{q_T}{h'_{t,3}} \frac{1}{1 - \frac{q_T}{h'_{t,3}}}\,. \tag{18}$$

Hence, the relative change of isentropic work depends on the ratio of the supplied specific heat to the apparent inlet total enthalpy. The amount of supplied heat depends on the thermal resistivity between the turbine casing and the exhaust gas and an accurate estimation is not possible without a heat transfer investigation. This usually leads to the development of Nusselt relations, which often require more input data than the method described here and remain typical for the investigated turbine casing due to its complexity. However, Figure 8 shows a typical trend for the heat transfer in the turbine of a passenger car turbocharger, whereby all values where normalized to unity. The results were obtained from measurements on manufacturer's hot gas test stand on three different turbochargers and heat flow analysis via Nusselt correlations and energy balance within the

control volumes of the test stand. All turbochargers were designed for a usage in passenger cars. The measurement and analysis methods are described in [13]. A higher shaft speed involves a higher mass flow (Figure 8, circles), hence, the flow velocity increases. As a result, the convective thermal resistivity reduces so that more heat is given off (triangles). However, the increase of the mass flow is steeper than that of the heat flow, hence, the specific supplied heat (squares) is lower at shaft speeds between $0.71u_{\max}$ and $u_{\max}$.

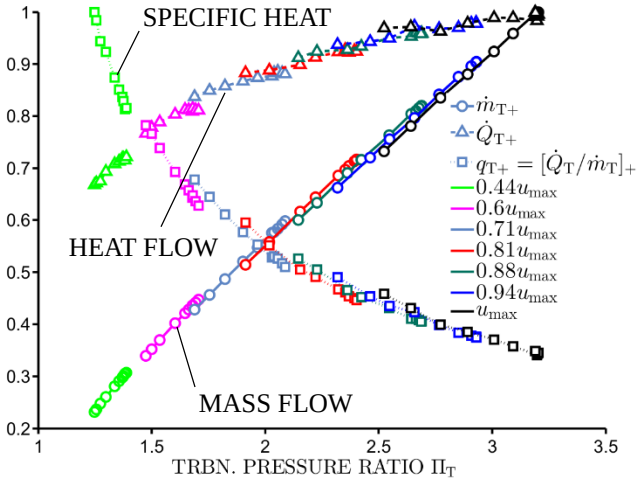

Figure 8. TYPICAL TURBINE MASS AND HEAT FLOW AT DIFFERENT SHAFT SPEED.

Since the inlet temperature of the exhaust gas is roughly constant while the kinetic energy at the measuring plane of manufacturers' test stand is negligible versus thermal energy, the inlet apparent total enthalpy is roughly constant and the ratio of specific heat to the latter may be a decreasing function of shaft speed as well. For all three investigated turbochargers between 1% and 10% of the total enthalpy was dissipated through heat, depending on the inlet temperature (higher ratio at higher inlet temperatures) and the shaft speed (lower ratio at higher shaft speeds).

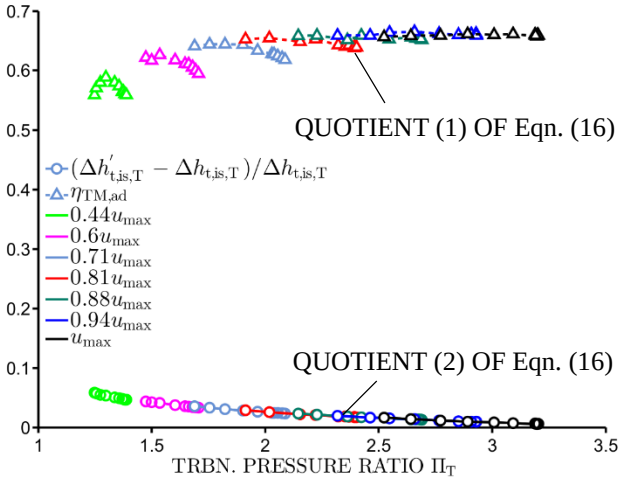

Figure 9. TYPICAL PATTERNS OF THE TWO COMPONENTS OF THE COMBINED EFFICIENCY SHIFT.

This may be the relevant value range for this ratio in turbocharger of the same size category. This is very low, so that according to Eqn. (18), the relative change of the isentropic work is approximately equal to the ratio of the supplied specific heat to the apparent inlet total enthalpy (see Figure 9, solid lines). The combined efficiency shift is then the product of two asymptotic patterns whereas one is an increasing and the other a decreasing function of the shaft with values between 1% and 10%. Both patterns are illustrated in Figure 9 and are typical for a small passenger car turbocharger.

Therefore, to determine the shift from the adiabatic to the real combined efficiency $\Delta\eta_{TM}$, a value for the ratio of the supplied specific heat to the total enthalpy at inlet between has to be assumed. It lies between 1% and 10% for the investigated turbo chargers. Then this value has to be multiplied with the mean value of the adiabatic combined efficiency from Eqn. (14).

IMPLEMENTATION AND VALIDATION

To validate the methods described in the two sections above, a turbocharger whose maps have already been calibrated with an engine that is mounted in a passenger car is used. The real compressor (Figure 13) and turbine maps (Figure 14) that arise from the application of these methods are compared to those of the manufacturer respectively in Figure 10 and Figure 11. It was assumed that the ratio of the specific heat dissipated prior to expansion in the turbine rotor to the total enthalpy of the exhaust gas at inlet is 8%. When comparing the apparent and the real compressor efficiency maps in Figure 10 and Figure 13 it is interesting to notice that there are no differences between the efficiencies of the three highest shaft speeds. Hence, the heat transfer effects at these speeds are negligible and a scaling is not necessary. The apparent efficiencies at lower speeds were shifted up through scaling in order to recover the real values.

From the real two dimensional maps, full three dimensional maps that are compatible with the control unit were computed. The computation method consist of interpolation and extrapolation of the available data points. Interpolation and extrapolation functions to predict the performance of the turbocharger have been presented in [14] and [15].

On board measurement were performed with manufacturers', real and calibrated maps. A car equipped with a two-stage turbocharger was available so that the boost pressure results from the product of the pressure ratios of low pressure (lp, first compression stage) and high pressure (hp, second compression stage) turbocharger. The scaling methods were only applied to the lp-turbocharger maps since the pre-compression from the latter may lead to further discrepancies between the manufacturer's and the real performance maps that were not discussed in this work, see [16]. Therefore, the feedback control of the lp stage was discarded while that of the hp-turbocharger was maintained. Particularly, the latter is required in dynamic situation such as acceleration from very low engine speeds because the lp is too sluggish in those cases. However, the main aim is to evaluate the capacity of the lp maps (i.e. manufacturer's [Figure 10 and Figure 11], real/scaled [Figure 13 and Figure 14] and calibrated maps) to match the desired boost pressure.

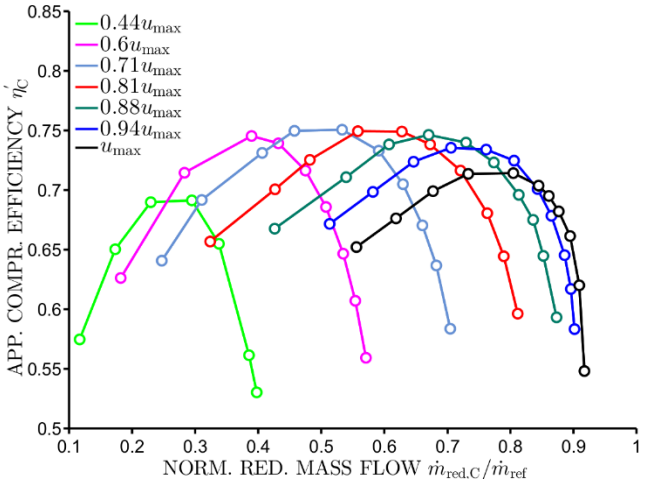

Figure 10. APPARENT COMPRESSOR EFFICIENCY.

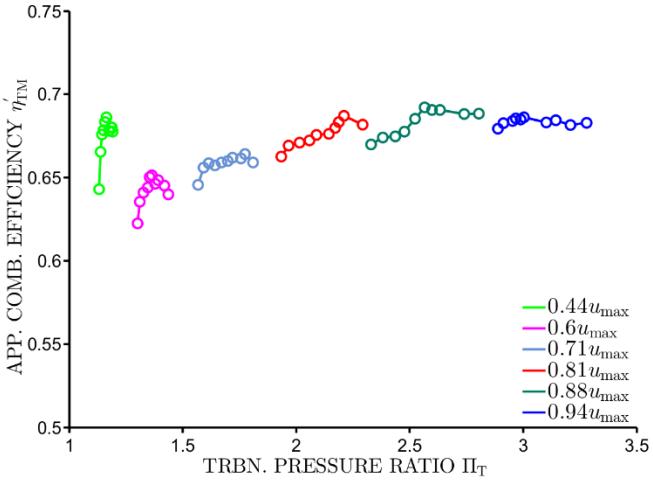

Figure 11. APPARENT COMBINED EFFICIENCY.

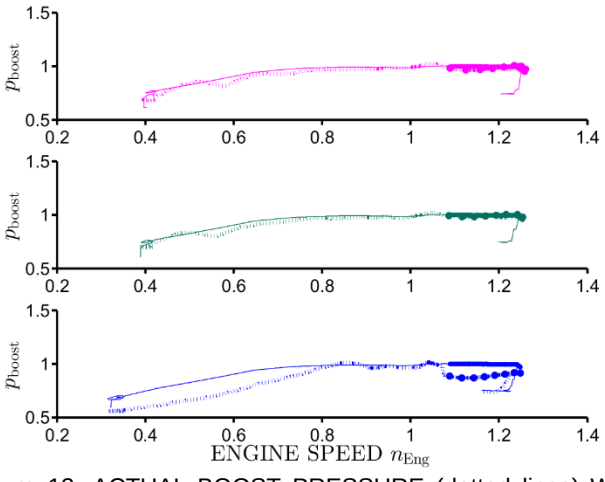

Figure 12. ACTUAL BOOST PRESSURE (dotted lines) WITH REAL (top), CALIBRATED (middle) AND MANUFACTURER'S (bottom) MAPS VERSUS DESIRED BOOST PRESSURE (solid lines) AT LOW INJECTION QUANTITY.

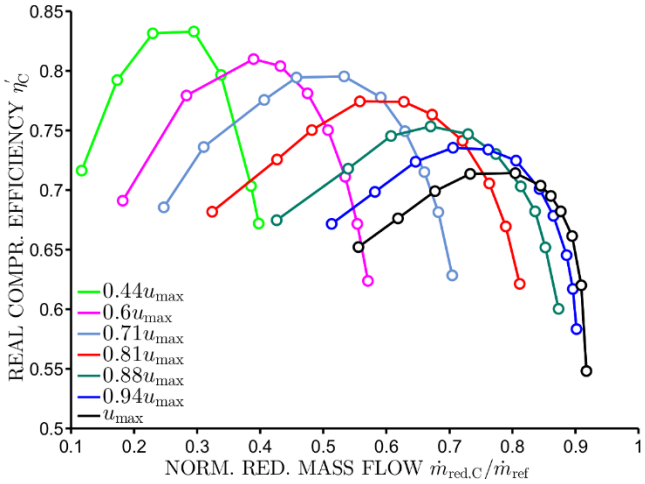

Figure 13. REAL COMPRESSOR EFFICIENCY.

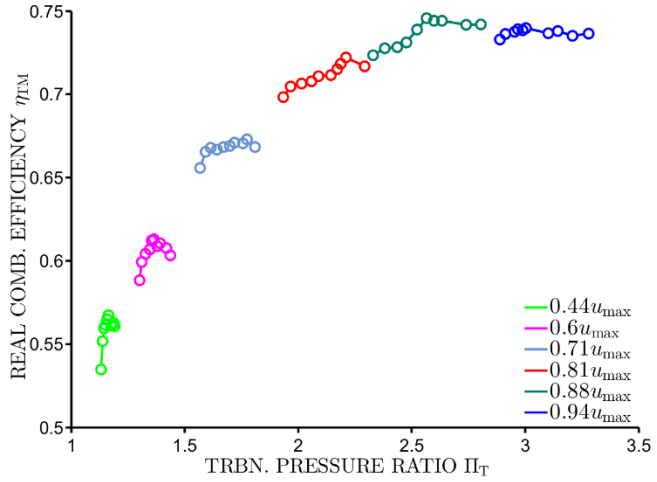

Figure 14. REAL COMBINED EFFICIENCY.

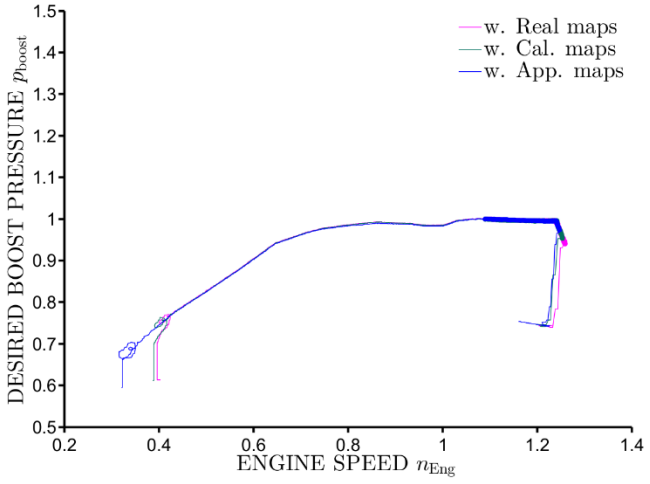

Figure 15. COMPARISON OF THE DESIRED BOOST PRESSURE FOR THE THREE MAPS AT LOW FUEL INJECTION RATE.

The results from the vehicle measurements are classified into two sections. The first one corresponds to the range where both the lp and the hp turbocharger contributes to the boost pressure rise. This is usually the case at the beginning of the measurement as explained above. The second section corresponds to the range where the boost pressure only results from the lp stage. In each measurement the injection quantity is set to be constant, i.e. constant vehicle load, and a steady increase of the engine speed was intended for all measurements.

Figure 12 shows the development of the outlet pressure over the engine speed for the three maps at a very low injection quantity (top for real maps, middle for calibrated maps and bottom for manufacturer's maps). The calibrated maps were already available in the test car and are not illustrated in this work.

The desired boost pressure is represented by solid lines and the actual boost pressure by dotted lines. The thinner lines represent the first section of the measurement where both turbochargers are involved in the boost pressure rise and the feedback control of the hp stage plays a dominant role. The ticker lines (solid and dotted) in each plot are more relevant for the interpretation of the results. They represent the second measurement section where the hp turbocharger is inactive and therefore, the actual boost pressure is equivalent to the outlet pressure of the lp compressor and is only controlled by the lp turbocharger maps provided. The boost pressure is normalized using the same value for all maps which is equal to the maximum value of the desired boost pressure in the second measurement section. The engine speed is normalized using the same constant value for all maps.

Figure 15 shows the engine operating point that is characterized using the engine speed and the desired boost pressure (since it characterizes the engine load together with the fuel injection rate). The desired boost pressure and the engine speed are normalized to unity as described above. The engine operating points during the measurement using the real turbocharger's efficiency maps are illustrated with purple lines, those using calibrated maps with green lines and those using manufacturer's maps with blue lines. As for Figure 12, the thin lines represent the first measurement section involving both turbochargers and the thick lines represent the second section involving only the low pressure turbocharger. All lines fall on each other, providing the evidence that the engine operating state is the same for all three measurements.

The main information from Figure 12 is that both boost control with real and calibrated maps are hugely satisfying while using manufacturers' maps doesn't fit well to the desired value. The accuracy of the boost control with real efficiency is even comparable with that of the calibrated maps. When the feedback control is inactive (sector with thicker lines in Figure 12) the discrepancies with manufacturer's maps are high while there is a good fit using calibrated and scaled maps. During the acceleration phase although the feedback control of the hp stage is activated the boost control with manufacturer's maps is still poor while the results with scaled maps are as good as those with calibrated maps. This emphasizes the assumption that the scaled maps are very close to the calibrated maps since the parameters of the feedback control may be specific to the engine-turbocharger-system available for the test.

The desired operating point of the lp compressor during the second measurement section are illustrated in Figure 16. Looking at the apparent and the real compressor efficiency maps in Figure 10 and Figure 13, it comes out that the desired operating points are in the range where both compressor and turbine maps were scaled.

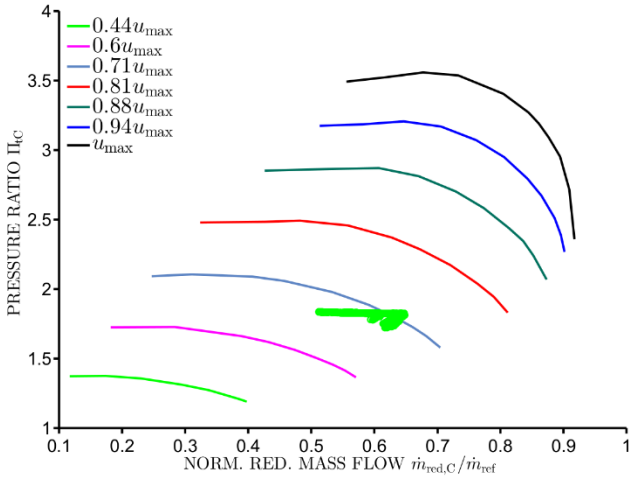

Figure 16. EVALUATED OPERATING POINTS OF THE LOW PRESSURE (LP) COMPRESSOR AT LOW INJECTION QUANTITY.

The results from another measurement at a higher fuel injection quantity are illustrated in Figure 17. As for the previous measurement, it comes out that the boost control with scaled maps is as good as with calibrated maps whereas using manufacturer's maps delivers less accuracy. However, the discrepancies with manufacturer's maps are lower than they were at lower injection quantity.

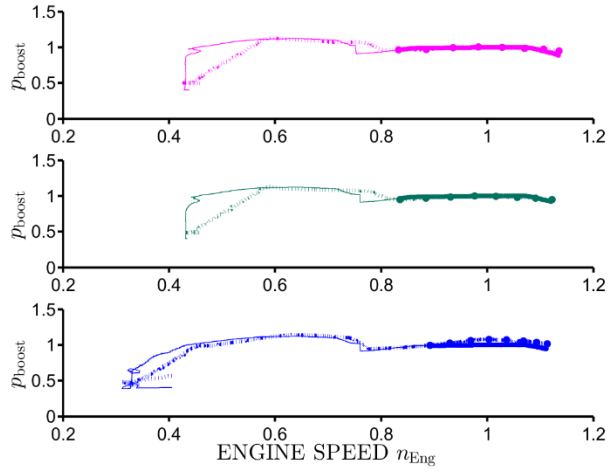

Figure 17. ACTUAL BOOST PRESSURE (dotted lines) WITH REAL (top), CALIBRATED (middle) AND MANUFACTURER'S (bottom) MAPS VERSUS DESIRED BOOST PRESSURE (solid lines) AT HIGH INJECTION QUANTITY.

In this Measurement the discrepancies at the beginning of the acceleration phase are not comparable since the same steady increase of the motor speed could not be achieved with all maps as illustrated in Figure 18.

The desired operating points of the lp compressor from the second measurement range are illustrated in Figure 19. All of them are in the range where the scaling of the compressor efficiency map is not necessary. Hence, the discrepancies are mainly due to the turbine heat transfer prior to expansion.

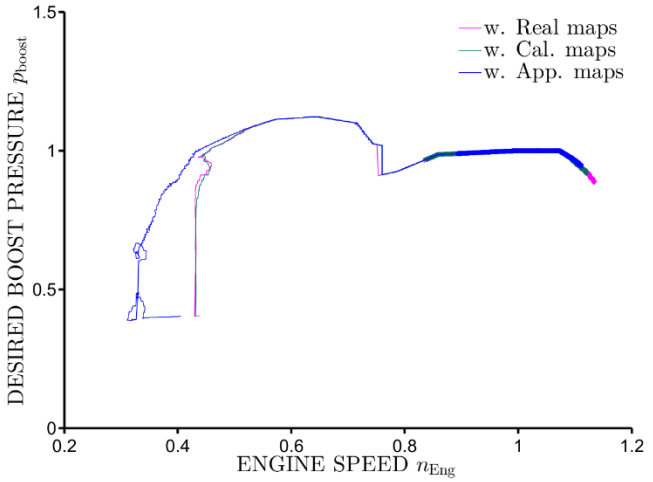

Figure 18. COMPARISON OF THE DESIRED BOOST PRESSURE FOR THE THREE MAPS AT HIGH FUEL INJECTION RATE.

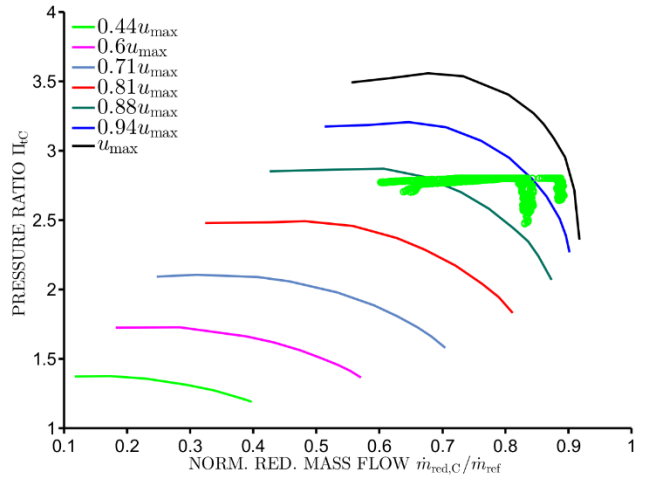

Figure 19. EVALUATED OPERATING POINTS OF THE LP COMPRESSOR AT HIGH INJECTION QUANTITY.

CONCLUSION

In this work, the scaling method proposed in [1] is used to counteract the heat transfer effects on the efficiency map of a compressor. A method to scale the turbine efficiency map based on the scaling method for the compressor map is proposed. It features a value for the ratio of the specific turbine heat to the turbine inlet total enthalpy that is estimated between 1% and 10% in the range of the investigated passenger car turbochargers. Through the methods described here, it is possible to acquire the real compressor and combined efficiency maps out of the apparent manufacturer's maps with less computational effort and without deep knowledge about the geometry of the turbocharger, the operating temperatures or the flow velocities.

The methods are applied on the maps of a turbocharger that is mounted on a passenger car. Vehicle measurements were performed and a comparison of the boost control using manufacturers', calibrated and scaled maps is done in order to validate the methods. The results clearly show that the boost control using manufacturer's maps is less accurate than that using calibrated or scaled maps, whereas the accuracy using these last two are comparable.

Starting from manufacturers' maps, calibrating the turbocharger maps is a time-consuming and costly process that is indeed systematic but does not fully exploit the potential of a model based control strategy. It has been shown that approximately the same control precision can be achieved through a simple, faster and physically based computation of the real maps as described in this work.

These methods are well suited for a single stage turbocharger and for the first stage of a two-stage turbocharging system. In the last case, further difficulties arise in the second stage compressor from the violation of the thermodynamic similarity as explained in [16]. This refers to the fact that the inlet state of the second stage compressor after pre-compression (in the first stage compressor) is considerably different than the inlet state that is displayed in manufacturers' maps. Further investigation of this issue is necessary in order to fully provide methods that are adequate for matching tasks in any single or multi-stage turbocharged engine.

REFERENCES

[1] Nakhjiri, M., Pelz, P. F., Matyschok, B., Däubler, L., Horn, A.: "Apparent and Real Efficiency of Turbochargers under Influence of Heat Flow", Isromac 14, Honolulu, 2012.

[2] Baines, M., Wygant, K., and Dris, A.: "The Analysis of Heat Transfer in Automotive Turbochargers", Proceedings of ASME Turbo Expo 2009, GT2009-59353, Orlando, 2009.

[3] Cormerais, M., Hetet, J.F., Chesse, P., and Maiboom, A.: "Heat Transfers Characterisation in a Turbocharger: Experiments and Correlations", Proceedings of ASME ICES 2006, ICES2006-1324, Aachen, 2006.

[4] Casey, M. V. and Fesich, T. M. (2010), "Efficiency of Turbocharger Compressors with Diabatic Flows", Journal of Engineering for Gas Turbines and Power, Vol. 132 / 072302-9, July 2010.

[5] Lüddecke, B., Filsinger, D. and Bargene, M., "On wide mapping of a mixed flow turbine with regard to compressor heat flows during turbocharger testing", Proceedings of the 10th International Conference on Turbochargers and Turbocharging (IMechE), pp. 185-202, 2011.

[6] Shaaban, S.: "Experimental Investigation and Extended Simulation of Turbocharger NonAdiabatic Performance", PhD Thesis, Universität Hannover, Hannover, 2004.
[7] Shaaban, S. and Seume, J.R.: "Analysis of Turbocharger Non-Adiabatic Performance", Proceedings of the 8th International Conference on Turbochargers and Turbocharging, pp. 119-130, London, 2006.
[8] Sirakov, B. and Casey, M. V., "Evaluation of Heat Transfer Effects on Turbocharger Performance", Proceedings of ASME Turbo Expo 2011, GT2011-45887, Vancouver, June, 2011.
[9] Pelz, P. F., Stonjek, S. and Matyschok, B. (2012), "The Influence of Reynolds Number and Roughness on the Efficiency of Axial and Centrifugal Fans – a Physically Based Scaling Method", Fan 2012 International Conference, 2012.
[10] Pelz, P. F. and Heß M., "Scaling Friction and Inertia Losses for the Performance Prediction of Turbomachines", Isromac-13, Honolulu, 2010.
[11] Rotzoll, R., "Untersuchungen an einer langsam-läufigen Kreiselpumpe bei verschiedenen Reynolds-Zahlen", Konstruktion im Maschinen-, Apparate- und Gebäudebau, 10/4, pp. 121-130, 1958.
[12] Payri, F., Serrano, J., Olmeda, P., Paez, A. and Vidal, F.: "Experimental Methodology to Characterize Mechanical Losses in Small Turbochargers", Proceedings of ASME Turbo Expo 2010, GT2010-22815, Glasgow, 2010.
[13] Nakhjiri, M., "Virtueller Turbolader auf Basis Physikalischer Modelle", unpublished research report, Technische Universität Darmstadt, 2014.
[14] El Hadef, J., Colin, G., Talon, V. and Chamaillard, Y.: "Physical Based Algorithms for Interpolation and Extrapolation of Turbocharger Data Maps", SAE Int. J. Engines, 2012.
[15] Moraal, P. and Kolmanovsky, I.: "Turbocharger Modeling for Automotive Control Applications", SAE 1999, 1999-01-0908.
[16] Nakhjiri, M., Pelz, P. F., Matyschok, B., Horn, A., "vATL – A Virtual Turbocharger on the Basis of Physical Models: Faster Calibration Processes with Deeper System Understanding", 9. Symposium Steuerungssysteme für automobile Antriebe, Berlin, 2012.
[17] Nakhjiri, M. and Pelz, P.F.: "Turbomachines under Periodic Admission – Axiomatic Performance Prediction", Proceedings of ASME Turbo Expo 2012, GT2012-68398, Copenhagen, June, 2012.

